Mode transition in dusty micro-plasma driven by pulsed radio-frequency source in C_2H_2/Ar mixture*

Xiang-Mei Liu(刘相梅)†, Rui Li(李瑞), and Ya-Hui Zheng(郑亚辉)

School of Science, Qiqihar University, Qiqihar 161006, *China*

(Received 22 October 2016; revised manuscript received 22 December 2016; published online 10 March 2017)

Physical qualities of dusty plasma in the pulsed radio-frequency C_2H_2/Ar microdischarges are carefully investigated by a one-dimensional hydrodynamic model and aerosol dynamics model. Since the thermophoretic force has a great effect on the nanoparticle density spatial distribution, the neutral gas energy equation is taken into accounted. The effects of pulse parameters (dust ratio, modulation frequency) on the nanoparticle formation and growth process are mainly discussed. The calculation results show that, as the duty ratio increases, the mode transition from the sheath oscillation (α regime) to the secondary electron heating (γ regime) occurred, which is quite different from the conventional pulsed discharge. Moreover, the effect of modulation frequency on the width of sheath and plasma density is analyzed. Compared with the H_2CC^- ions, the modulation frequency effect on the nanoparticles density becomes more prominent.

Keywords: pulsed process parameters, C_2H_2/Ar microdischarges, dusty plasma

PACS: 52.27.Lw, 52.65.–y **DOI:** 10.1088/1674-1056/26/4/045202

1. Introduction

Hydrogenated amorphous carbon (α-C:H) thin films deposited by the plasma enhanced chemical vapor deposition (PECVD), is widely used in passivation layers[1] and flat-screen displays.[2] In PECVD, the formation and growth of nanoparticles is a generally recognized problem. It turns out to be harmful in the microelectronics industry,[3,4] whereas in nanoscale materials, it is beneficial.[5] To describe the nanoparticles formation and growth mechanism clearly, Deschenaux *et al.*[6] studied the radio frequency (RF) acetylene dusty plasma by using mass spectrometry. The mass spectrometry showed that the higher-mass hydrocarbon anions and cations nearly 200 amu is formed from the species comprising 14–15 carbon atoms. In theory research, De Bleecker *et al.*[7,8] developed a detailed chemical kinetic scheme to reveal the nanoparticle formation mechanisms in RF acetylene plasma. However, their results for negative ions are not in agreement with the experiment by Deschenaux.[6] Thus, Mao *et al.*[9] extend De Bleecker's one-dimensional fluid model by adding some new mechanisms for negative ion formation. When comparing with the experiment results,[6,10] a reasonable agreement is received. However, in these studies the thermophoretic force is not taken into account for the constant gas temperature. It has been shown that, thermophoretic force has a great affect on the spatial distribution of nanoparticles,[11] thus the neutral gas energy equation should be considered.

In PECVD, to obtain better uniformity and higher deposition rate, atmospheric pressure RF acetylene discharges is often used. In recent years, microdischarges (MDs) have received extensive attention due to their specific advantages, such as stable non-equilibrium, highly energetic electrons, and different discharge structures characteristics. Thus, they are widely used in materials treatment and modification, microsatellite propellers, and plasma display panels.[12,13] In MDs, the pressure is generally very high while the plate distances are in the range of micrometer and submillimeter, thus the secondary electron emission play a dominant role. However, when the discharge conditions are slightly changed, the stable non-equilibrium plasma is easy to convert to non-uniform discharge. These shortcomings have greatly restricted the application of MDs. But fortunately, the recent studies have indicated that, MDs driven by pulse source instead of the conventional AC discharge can obtain uniform plasma in a larger parameter range.[14] Pulsed discharges have received extensive attention due to their advantages, such as the higher peak current density, electron density and electron generation efficiency, the easier to produce the uniform large area plasma, and the higher nonbalance of the generated plasma.[15–19] Therefore, it is necessary to investigate nanoparticles formation and growth mechanism and pulsed discharge mode in RF acetylene microdischarge.

In this article, we mainly studied the behavior of nanoparticles in C_2H_2/Ar pulsed radio-frequency MDs plasma, which are generally produced by a series of chemical reactions.[20,21] The fluid model[9] is extended by adding the neutral gas flow and heat transfer equations, thus the role of thermophoretic

*Project supported by the Natural Science Foundation of Heilongjiang Province, China (Grant Nos. A2015011 and A2015010), the Postdoctoral Scientific Research Developmental Fund of Heilongjiang Province, China (Grant No. LBH-Q14159), the National Natural Science Foundation of China (Grant Nos. 11404180 and 11405092), and the Program for Young Teachers Scientific Research in Qiqihar University, Heilongjiang Province, China (Grant No. 2014kZ11).

†Corresponding author. E-mail: lxmjsc98@163.com

© 2017 Chinese Physical Society and IOP Publishing Ltd

force on the nanoparticles formation and growth mechanism is presented. The effects of pulse width, repetition frequency on electrons, ions, radicals as well as nano particles densities, electron temperature, plasma uniformity are our mainly concerned. The outline of the paper is presented as follows: Section 2 summarizes the fluid model and the aerosol dynamics model, and analyzes the simulation conditions of those models. In Section 3, the pulsed discharge parameters effects on the plasma property and nanoparticles behavior are carefully investigated, and some brief conclusions are presented in the end of paper.

2. Theoretical model

2.1. Fluid model

Fluid models solve the continuity equations for each species j including electrons, ions, radicals, neutral gases, and nanoparticles[20,21] in the C_2H_2/Ar MDs plasma is described by

$$\frac{\mathrm{d}n_j}{\mathrm{d}t}+\frac{\mathrm{d}\Gamma_j}{\mathrm{d}x}=R_j, \tag{1}$$

where n_j is particle density, R_j represents the source and sink terms. The particle flux terms Γ_j for electrons, ions and radicals are given by

$$\Gamma_j=\mu_j n_j E_j-D_j\frac{\mathrm{d}n_j}{\mathrm{d}x}. \tag{2}$$

where μ_j and D_j are mobility and diffusion coefficient for particles j. Since the masses for ions are much larger than that of electrons, the effective electric field is introduced to follow the inertia effects. For nanoparticles, the flux equation is determined by the assuming that the neutral drag force balances with the sum of electrostatic force, ion drag force and thermophoretic force

$$\begin{aligned}\Gamma_\mathrm{d}=&-\mu_\mathrm{d}n_\mathrm{d}E_\mathrm{eff}-D_\mathrm{d}\frac{\mathrm{d}n_\mathrm{d}}{\mathrm{d}x}-\frac{n_\mathrm{d}}{v_\mathrm{md}}g\\&+\sum\frac{n_\mathrm{d}m_\mathrm{i}\upsilon_\mathrm{s}}{m_\mathrm{d}v_\mathrm{md}}\left(4\pi b_{\pi/2}^2\Gamma+\pi b_\mathrm{c}^2\right)\Gamma_i\\&-\frac{32}{15}\frac{n_\mathrm{d}r_\mathrm{d}^2}{m_\mathrm{d}v_\mathrm{md}\upsilon_\mathrm{th}}k_\mathrm{T}\frac{\mathrm{d}T_\mathrm{gas}}{\mathrm{d}x}.\end{aligned} \tag{3}$$

Here n_d and Γ_d are the density and flux for nanoparticles. m_i and m_d are the ion mass and nanoparticle mass, respectively. g is the gravitational acceleration and k_T the thermal conductivity. υ_s and υ_th are the ion average speed and average thermal velocity. v_md represents momentum loss frequency and Γ the Coulomb logarithm. The transport equation is incorporated in each nanoparticle domain of aerosol dynamics model (Subsection 2.2), the nanoparticle between 1.0 nm and 50 nm in diameter is taken into consideration.

The neutral gas temperature T_gas is not taken as a constant, and calculated by

$$\frac{\partial}{\partial t}(n_\mathrm{n}C_\mathrm{v}T_\mathrm{gas})+\nabla\cdot(n_\mathrm{n}C_\mathrm{v}T_\mathrm{gas}\boldsymbol{u}_\mathrm{n})=-\nabla\cdot\boldsymbol{q}_\mathrm{n}-p_\mathrm{n}\nabla\cdot\boldsymbol{u}_\mathrm{n}+E_\mathrm{n}, \tag{4}$$

where n_n and $\boldsymbol{q}_\mathrm{n}$ are the density and heat flux vector for neutral gases, respectively. E_n represents energy transfer to the neutral species by collisions with other species. C_v is the heat capacity at constant volume. The neutral gas velocity $\boldsymbol{u}_\mathrm{n}$ is described by

$$\frac{\partial n_\mathrm{n}m_\mathrm{n}\boldsymbol{u}_\mathrm{n}}{\partial t}+\nabla\cdot(n_\mathrm{n}m_\mathrm{n}\boldsymbol{u}_\mathrm{n}\boldsymbol{u}_\mathrm{n})=-\nabla p_\mathrm{n}-\nabla\cdot\overrightarrow{\overrightarrow{\Pi}}_\mathrm{n}+\boldsymbol{M}_\mathrm{n}, \tag{5}$$

where p_n and m_n are the gas pressure and mass for the neutral gases. $\boldsymbol{M}_\mathrm{n}$ is the transfer of mass to the neutral gas fluid by collisions with other species. $\overrightarrow{\overrightarrow{\Pi}}_\mathrm{n}$ is the neutral viscous stress tensor.

To obtain electric fields, Poisson's equation is coupled with the continuity and momentum equations, make the fluid model self-consistent. Finally, the electrons energy balance equations are solved to determine the electron temperature, while the ion pressure take a little role in the momentum equation, thus the ion temperature is set at a constant of 400 K. The discharge parameters, such as the diffusion constants and mobility as well as the electron collisions (ionization, attachment, and dissociation) coefficients as a function of the average electron energy, are calculated from the electron energy distribution function (EEDF). The EEDF are obtained from the Boltzmann equation in a two-terms approximation. Consequently, the particle density, potential, electron temperature, neutral gas temperature and the other characteristics of plasmas can be described as a function of position, owing to the correlation of each equation.

2.2. Aerosol dynamics model

The aerosol dynamics model in this article is used to investigated the nanoparticles growth process. In the model, the temporal evolution of the nanoparticles density $n(v)$ in a volume range $(v, v+\mathrm{d}v)$, can be investigated by the general dynamic equation.[22]

$$\begin{aligned}\frac{\partial n(v)}{\partial t}=&\frac{1}{2}\int_0^v\beta(u,v-u)n(v-u)n(u)\,\mathrm{d}u\\&-\int_0^\infty\beta(u,v)n(v)n(u)\,\mathrm{d}u+J_0(v)\delta(v-v_0),\end{aligned} \tag{6}$$

where the first term on the right-hand side accounts for the particles formation between two smaller particles owing to the coagulation, while the second term expresses the loss of particles from coagulation with all particles. The third term is the new particles formation, where the formation rate with volume v_0 from nucleation is $J_0(v)$. The factor 1/2 in the first term on the right-hand side is used to avoid collisions counted twice in the integral, $\beta(u,v)$ is the coagulation frequency between interacting particles with volume u and volume v. In this computation, the volume domain was divided logarithmically in

38 sections, comprising particles between 1.0 nm and 50 nm in diameter.

The primary large anions of nanoparticles formation in this C_2H_2/Ar MDs plasma is the $C_{12}H^-$ and $C_{12}H_2^-$, which are produced by successive anion-C_2H_2 polymerization reactions,

$$\begin{aligned} C_2H_2 + C_{2n}H^- &\rightarrow C_{2n+2}H^- + H_2, \\ C_2H_2 + C_{2n}H_2^- &\rightarrow C_{2n+2}H_2^- + H_2, \end{aligned} \tag{7}$$

where the larger anions $C_{2n+2}H^-$ and $C_{2n+2}H_2^-$ are primarily formed by C_2H^- and H_2CC^-. To simplify the calculation, two different pathways are all stopped at anions containing 12 carbon atoms in the model, as we couldn't describe an unlimited number of larger anions ($C_{2n+2}H^-$ and $C_{2n+2}H_2^-$). The aerosol dynamics model is finally coupled to the fluid model to describe the formation and growth mechanisms of nanoparticles.

2.3. Boundary conditions

In this work, the RF sources 13.56 MHz is applied to the upper electrode, while the lower electrode is grounded. The boundary conditions for the fluid model specified are as follows:[23] the electron flux at the electrodes is describe by

$$\Gamma_e = \frac{1}{4} n_e \upsilon_{th,e} (1 - \Theta) + \gamma \Gamma_i$$

with the electron reflection coefficient $\Theta = 0.25$, the secondary electron emission coefficients $\gamma = 0.1$. Similar to the electron flux, the negative ion flux

$$\Gamma_- = \frac{1}{4} n_- \upsilon_{th,i},$$

and the positive ion flux gradients at the electrodes $\partial \Gamma_+ / \partial x = 0$. The neutral gas velocity gradients at the electrodes $\partial n_n / \partial x = 0$. The radicals flux at the electrode is

$$\Gamma_n = \frac{s_i}{2(2 - s_i)} n_n \upsilon_{th},$$

where the sticking probability of radicals s_i is given by Ref. [7].

2.4. Simulation conditions

In this article, one-dimensional fluid model and aerosol dynamics model are used to investigate the nanoparticles behavior in pulsed radio-frequency C_2H_2/Ar MDs plasma between two parallel palates. The discharge conditions of these model are as follows: the size of parallel-plate reactor is 500 μm, the total gas pressure is 600 Torr (1 Torr = 1.33322 × 10^2 Pa), the proportion of Ar concentration is set at 95% to ensure the stable non-equilibrium plasma in microdischarges, the ion temperature $T_{ion} = 400$ K. Since the neutral gas energy balance equation is taken into account, the total gas flow rate is set at $F_{tot} = 400$ sccm, and C_2H_2 accounts for 5% of the total flow rate. In this model, 2000 time steps per RF cycle and 100 grid points are used, means that the time step is $T_{RF}/2000$. Since the masses of neutral particles and dust particles are much larger than that of electrons, a longer time step of $T_{RF}/20$ is used for describing the neutral–neutral chemistry and $5T_{RF}$ is used for describing dust particles.

3. Results and discussion

In this article, we mainly investigated the physical qualities of dusty plasma in pulsed radio-frequency C_2H_2/Ar MDs, thus the influences of duty ratio, modulation frequency on the electron density, H_2CC^- density, and nanoparticles density are carefully discussed.

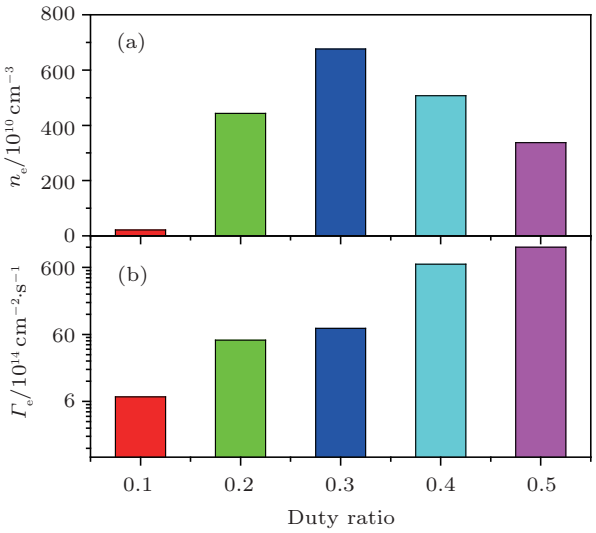


Fig. 1. (color online) The variation of electron density n_e at the center of the discharge and electron flux Γ_e at upper electrode, with duty ratio $\eta = 0.1$, 0.2, 0.3, 0.4, and 0.5.

Figure 1 illustrates the variation of electron density at the center of the discharge and the electron flux at the upper electrode, with the duty ratio $\eta = 0.1, 0.2, 0.3, 0.4, 0.5$. As we can be seen, a maximum point for electron density is presented at duty ratio $\eta = 0.3$. That is to say, the electron density increases definitely with the increasing of duty ratio in the range of $0.1 \sim 0.3$, while decreases with the increasing of duty ratio in the range of $0.3 \sim 0.5$. The most likely cause of this phenomenon is that a mode transition appears around the duty ratio $\eta = 0.3$. When the duty ratio is less than 0.3, the discharge is mainly sustained by the sheath capacitance. Although some ionization does produced by the high-energy secondaries, the electron current is very small comparing with the ion current. Therefore, most of the secondary electrons are lost from the discharge before significant ionization occurs, and then sheath oscillation is responsible for sustaining discharge (α regime). However, as the duty ratio increases from 0.3 to 0.5, electron current increases rapidly, which has been shown in Fig. 1(b), and then secondary electrons are responsible for the significant ionization (γ regime). On the other hand, increased the duty

ratio tends to reduce the sheath depth, which cause the secondary electrons emitted from the electrodes decrease. Thus, the electron density decreases with the increasing of duty ratio in the range of $0.3 \sim 0.5$.

The negative ion H_2CC^- density variation with the duty ratio is described in Fig. 2. As is well known in Refs. [9] and [24], 95% of the carbon nanoparticles formation and growth was triggered by the reactive H_2CC^- precursor. Thus, the duty ratio effects on the H_2CC^- density should be carefully studied. For the same reason as the changing trend of electron density, we can clearly see that the H_2CC^- density first increases and then decreases with the increasing of duty ratio, and it is generally at a rather high value (10^{12} cm^{-3}). This calculation results have once again provided evidence for the existence of the mode transformation (α to γ).

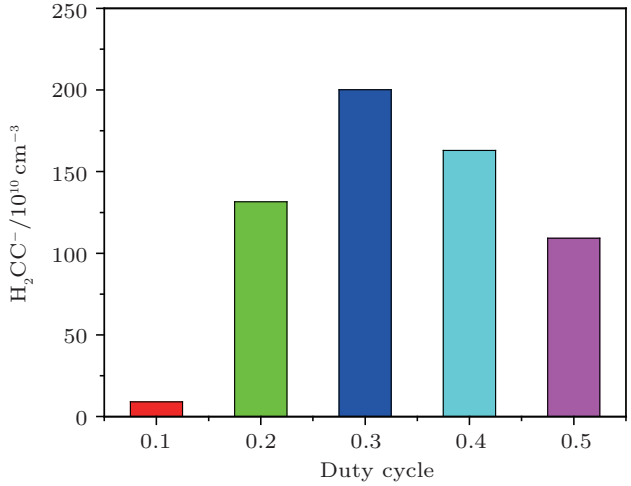


Fig. 2. (color online) he variation of negative ion (H_2CC^-) at different electrode spacings, with the settings being the same as those in Fig. 1.

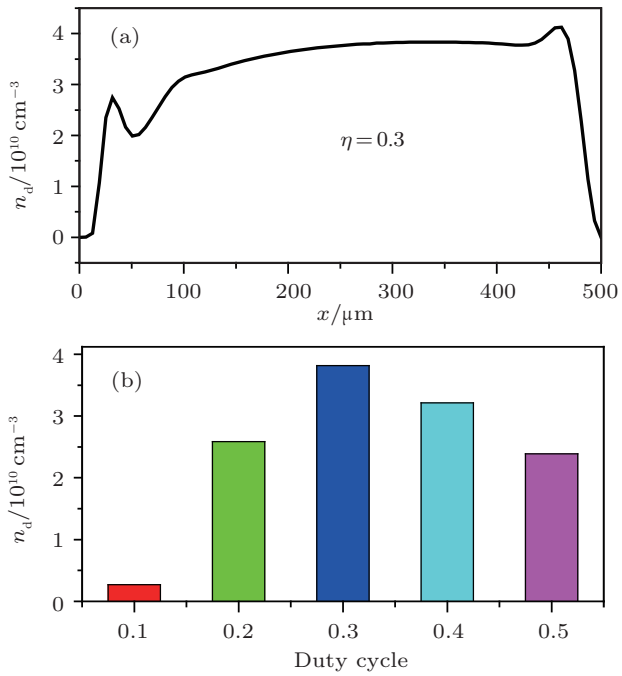


Fig. 3. (color online) The variation of nanoparticles number density n_d at different electrode spacings, with the same settings as those in Fig. 1.

In order to investigate the behavior of nanoparticles clearly, figure 3(a) shows the spatial variation profile of nanoparticle density at the duty ratio $\eta = 0.3$ and figure 3(b) shows the nanoparticle density at the center of the discharge at different duty ratio, with the nanoparticle diameter $D_d = 10$ nm. It can be clearly seen from Fig. 33(a) that, the nanoparticle exhibits a local maximum near the showerhand electrode under the influence of thermal gradient in gas temperature, and keeps much higher value in the bulk plasma, owing to the larger collisions frequency at gas pressure of 600 Torr. In addition, we also can see from Fig. 3(b) that, the nanoparticle density shows a rapid increase in the duty ratio range of 0.1 and 0.3, while a gentle decrease in the range of 0.3 and 0.5. The maximum of nanoparticle density 4×10^9 cm^{-3} is appeared at the duty ratio $\eta = 0.3$.

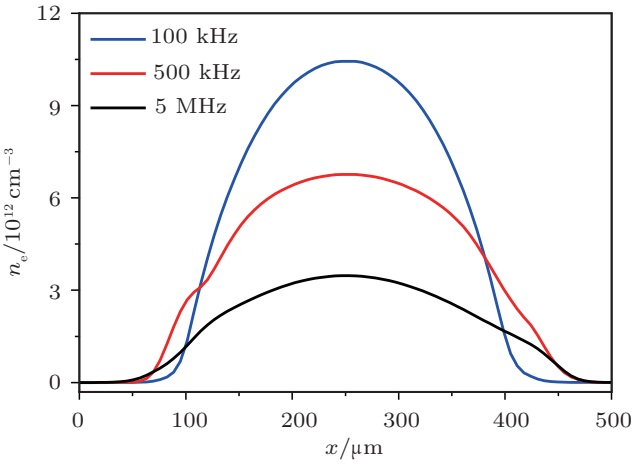


Fig. 4. (color online) The spatial variation profiles of electron density n_e at different electrode spacings, with the modulation frequencies $f = 100$ kHz, 500 kHz, and 5 MHz.

Figure 4 displays the spatial variation profiles of electron density in a pulse period, with the modulation frequencies $f = 100$ kHz, 500 kHz, and 5 MHz while the duty ratio is fixed at a certain value $\eta = 0.3$ throughout our calculations. It is clearly seen in Fig. 4 that the electron density responds strongly to the modulation frequency. The electron density increases from approximately 3×10^{12} cm^{-3} at $f = 5$ MHz to a maximum of approximately 11×10^{12} cm^{-3} at $f = 100$ kHz. In general the following two main reasons can be used to explain this phenomenon.

(i) The width of sheath becomes broader with the decrease of the modulation frequency, and then the secondary electrons emitted from the electrodes increase. Therefore, the electron density varies significantly with the modulation frequency.

(ii) As the modulation frequency gets lower, the pulse-on time increases,[20] which resulting in larger collisions rate. The collision effect in the sheath region drives the electron density increases.

Thus, we can conclude that adjustments of modulation frequency can be an effective method for electron density increasing.

Figure 5 shows the spatial variation of negative ion H_2CC^- density in a pulse period, with the modulation frequency presented at three different values. We can see in Fig. 5 that H_2CC^- density increases from approximately 5×10^{11} cm^{-3} to a maximum of approximately 9×10^{11} cm^{-3} with the decreasing of modulation frequency. It can be also seen that, upon changing the modulation frequency, the sheath width increase slightly. This is the reason why the negative ion H_2CC^- density just increased by two times with the decreasing of modulation frequency, compared with the electron density.

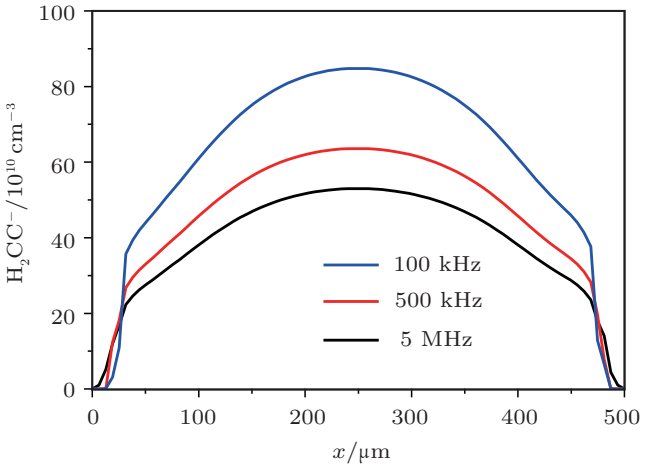


Fig. 5. (color online) The spatial variation profiles of negative ion (H_2CC^-) density at different electrode spacings, with the same settings as those in Fig. 4.

The effect of modulation frequency on the nanoparticle density is also taken into accounted, as shown in Fig. 6. The nanoparticle density has been time averaged in a pulse period, and the nanoparticle diameter is chosen at $D_d = 10$ nm. We can see in Fig. 6 that the nanoparticle density in the plasma bulk increases with the decreasing of modulation frequency, which brings about a two-fold increase. However, the nanoparticle density near the showerhand electrode is significantly increased from approximately 1×10^{10} cm^{-3} at $f = 5$ MHz to a maximum of approximately 8×10^{10} cm^{-3} at $f = 100$ kHz. There are three reasons listed below for this phenomenon.

i) A greater thermal gradient in gas temperature is presented near the showerhand electrode, which make the nanoparticle density exhibits a local maximum near the showerhand electrode.

ii) The sheath width increases greatly with the decreasing of the modulation frequency, which cause the nanoparticle density near the showerhand electrode increase rapidly.

iii) The initial particle H_2CC^- density of nanoparticle formation increases slightly with the decreasing of the modulation frequency, resulting that the nanoparticle density in bulk plasma region changed less.

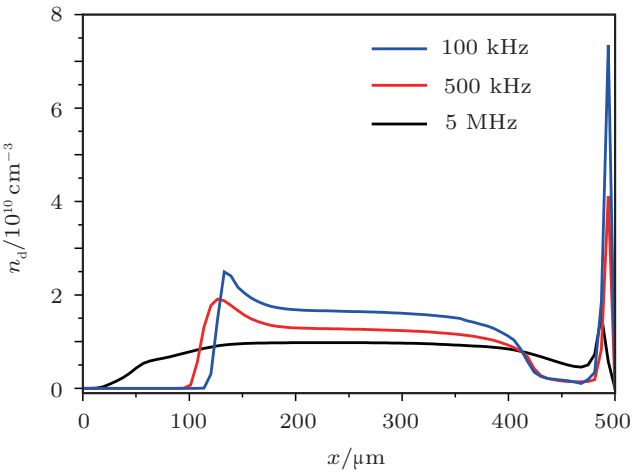


Fig. 6. (color online) The spatial variation profiles of nanoparticles number density n_d at different modulation frequencies, with the same settings as those in Fig. 4.

4. Conclusion

In conclusion, the effects of pulse parameters on the formation and growth of dust particles are investigated in pulsed radio-frequency microdischarges plasma by using a self-consistent couple of aerosol dynamics model and fluid model. The aerosol dynamics model is used to determine the nanoparticles growth process, and the fluid model is used to determine the nanoparticles formation process and calculate the spatiotemporal evolution of electrons, ions, and neutrals. In the simulation, the neutral gases energy equation is taken into account.

Different from what we have learned in pulsed discharge, a mode transition from electron collision heating (α regime) to secondary electron heating (γ regime) has been found as the duty ratio increases from 0.1 to 0.5, basing on the variation of electron density, H_2CC^- density and nanoparticles density. When the duty ratio is less than 0.3, comparing with the ion current, the electron current is very small, thus sheath oscillation is responsible for sustaining discharge. As the duty ratio increases, the electron current increases, secondary electrons are sufficient for the significant ionization. The modulation frequency effects on the plasma density are also discussed. By decreasing the modulation frequency, the width of sheath increases, the electron density, H_2CC^- density and nanoparticles density increase rapidly, especially the nanoparticles density near the showerhand electrode. Furthermore, the results show that the neutral gas temperature gradient has a great effect on the spatial distribution of nanoparticle density.

References

[1] Daniels B K, Brown D W and Kimock F M 1997 *J. Mater. Res.* **12** 2485
[2] Robertson J 2002 *Mater. Sci. Eng. R.* **37** 129
[3] Xu N S and Huq S E 2005 *Mater. Sci. Eng. R: Rep.* **48** 47
[4] De Bleecker K, Bogaerts A, Gijbels R and Goedheer W 2004 *Phys. Rev. E* **69** 056409
[5] Ostrikov K 2005 *Rev. Mod. Phys.* **77** 489
[6] Deschenaux Ch, Affolter A, Magni D, Hollenstein Ch and Fayet P 1999 *J. Phys. D: Appl. Phys.* **32** 1876
[7] De Bleecker K, Bogaerts A and Goedheer W 2006 *Phys. Rev. E* **73** 026405
[8] De Bleecker K, Bogaerts A and Goedheer W 2006 *Appl. Phys. Lett.* **88** 151501
[9] Mao M, Benedikt J, Consoli A and Bogaerts A 2008 *J. Phys. D: Appl. Phys.* **41** 225201
[10] Benedikt J, Consoli A, Schulze M and von Keudell A 2007 *J. Phys. Chem. A* **111** 10453
[11] Moravej M 2006 *Plasma Sourcs Sci. Technol.* **15** 204
[12] Kogelschatz U 2007 *Contrib. Plasma Phys.* **47** 80
[13] Munoz-Serrano E, Hagelaar G, Callegari Th, Boeuf J and Pitchford L C 2006 *Plasma Phys. Control. Fusion* **48** B391
[14] Lieberman M A and Lichtenberg A J 2005 *Principles of Plasma Discharges and Materials Processing*, 2nd edn. (New York: Wiley-Interscience)
[15] Pai D, Stancu G, Lacoste D and Laux C 2009 *Plasma Sources Sci. Technol.* **18** 045030
[16] Ito T, Kobayashi K, Czarnetzki U and Hamaguchi S 2010 *J. Phys. D: Appl. Phys.* **43** 062001
[17] Lu X and Laroussi M 2006 *J. Phys. D: Appl. Phys.* **39** 1127
[18] Laroussi M, Lu X, Kolobov V and Arslanbekov R 2004 *J. Appl. Phys.* **96** 3028
[19] Pai D, Lacoste D and Laux C 2010 *J. Appl. Phys.* **107** 093303
[20] Liu X M, Li Q N and Xu X 2014 *Chin. Phys. B* **23** 085202
[21] Liu X M, Li Q N and Li R 2015 *Chin. Phys. B* **24** 075204
[22] Iza F, Lee J K and Kong M G 2012 *Phys. Rev. Lett.* **99** 075004
[23] Boeuf J P and Pitchford L C 1995 *Phys. Rev. E* **51** 1376
[24] Wetering F, Beckers J and Kroesen G 2012 *J. Phys. D: Appl. Phys.* **45** 485205